Laser precession machining of cross-shaped terahertz bandpass filters

Le, Hoang; Pradhani, Chandra; Penchev, Pavel; Nasrollahi, Vahid; Karkantonis, Themistoklis; Wang, Yi; Dimov, Stefan; Ramos-de-Campos, Jose

DOI:
10.1016/j.optlaseng.2021.106790

Document Version
Peer reviewed version

Citation for published version (Harvard):
Le, H, Pradhani, C, Penchev, P, Nasrollahi, V, Karkantonis, T, Wang, Y, Dimov, S & Ramos-de-Campos, J 2022, 'Laser precession machining of cross-shaped terahertz bandpass filters', *Optics and Lasers in Engineering*, vol. 149, 106790. https://doi.org/10.1016/j.optlaseng.2021.106790

Laser precession machining of cross-shaped terahertz bandpass filters

Hoang Le[a], Chandrasekhar Pradhani[b], Pavel Penchev[a], Vahid Nasrollahi[a], Themistoklis Karkantonis[a], Yi Wang[b], Stefan Dimov[a], Jose A. Ramos-de-Campos[c].

[a] Department of Mechanical Engineering, University of Birmingham, UK.

[b] Department of Electronic, Electrical and Systems Engineering, University of Birmingham, UK.

[c] LASEA S.A., Liège Science Park, Rue Louis Plescia 31, 4102 Seraing, Belgium.

Corresponding author: Hoang Le

Email address: hxl683@student.bham.ac.uk

Abstract

The laser micro-machining technology is an attractive alternative to conventional photoresist-based technologies for manufacturing terahertz (THz) cross-shaped mesh filters. It can address some limitations related to filter's quality, process complexity, unit cost and available materials. However, there are also open issues associated with the laser micro-machining technology that have to be addressed. In particular, some intrinsic characteristics of laser micro-machined structures, i.e. the side-wall tapering, that impact both achievable geometrical and dimensional accuracy and the filters' performance. This research proposes a novel fabrication process, called laser precession machining, that addresses some of the key laser micro-machining limitations in producing THz mesh filters. It employs an ultrafast laser and a "precess" module to vary the beam incident angle and thus to minimise the taper angle on the sidewalls of the filters' cross-shaped through holes. A significant reduction of this negative tapering effect was achieved on micro-structures produced with this new method that led to a significant improvement of filters' performance. The filters' performance was compared with the simulation results and they were in good agreement. X-ray photoelectron spectroscopy (XPS) analysis was carried out to analyse the effects of laser precession machining on the composition of copper substrates as a potential factor affecting the filters' performance.

Keywords: Terahertz, Cross-shaped, Mesh Filter, Laser Micro-machining, Precession, Tapering Effect.

1. Introduction

The interests in developing and implementing terahertz (THz) technology have been growing consistently in the last decade with a wide range of applications offering unique capabilities [1]. The THz emission frequency covers the gap between the microwave and infrared radiation in the electromagnetic spectrum, ranging from 0.1 to 10 THz that is equivalent to wavelength from 3 mm to 30 μm and exists in non-ionizing form [2, 3]. Applications of the terahertz radiation can be found in various areas, such as biomedical imaging, cancer detection, food and water inspection, radars, security and astronomy [4-9]. One of the key components in many THz communication systems are the frequency restricting components that act as filters in selecting one or more target frequency bands [10, 11]. A typical example of such components are the frequency selective surfaces which are formed of two-dimensional arrays of through structures onto a thin substrate, also known as mesh filters [12]. One popular through structure of the THz mesh filters are cross-shaped holes with critical dimensions such as length, width and periodicity [13, 14]. Consequently, the performance of cross-shaped THz

mesh filters is very sensitive to their geometrical accuracy [15]. Therefore, the technologies used for their manufacture normally require a very high accuracy and repeatability [16].

Photolithography that employs SU-8 photoresist has been used to manufacture THz components and frequency selective surfaces [17, 18]. This technology typically produces components with a very high geometrical accuracy, especially in regard to the taper angle on the micro-structures' sidewall, that affects the mesh filters' performance. This is an important prerequisite for achieving a good mesh filter's performance, i.e. transmitting only the selected frequencies with minimum insertion losses, as these THz device's characteristics are very sensitive to any dimensional variations. However, photolithography also has some intrinsic shortcomings, in particular it can only process photoresist materials with their limited mechanical, thermal and electrical properties. SU-8 is an epoxy-based photoresist with Young's modulus in range of 2.92 to 4.95 GPa that is far lower when compared with metallic substrates [19]. In addition, SU-8 has a high electrical resistivity and therefore the photoresist-based manufacturing technologies for producing THz devices have to include a metallisation step.

There are other manufacturing technologies of producing frequency selective surfaces such as electron-beam lithography, nanoimprint lithography, deep reactive ion etching and inkjet printing [20-22]. These technologies again require an additional metallisation step, as with the case of photolithography. Hard substrates are usually required to reinforce the mesh filters fabricated with them. Another common limitation of these technologies is that they are capital intensive and therefore are mostly viable for relatively large batch sizes while the unit costs are still relatively high due to the use of clean room manufacturing technologies.

In this context, laser-based micro machining offers unique advantages compared to photoresist-based manufacturing technologies, especially for producing THz frequency selective surfaces. It is a direct write and non-contact process and can be used to structure almost any material [23]. Therefore, the researchers have started looking at employing this technology for fabricating THz communication components [24-28].

Table 1 compares the capabilities of photoresist-based technologies against laser-based ones for producing THz devices. It can be clearly seen that laser-based micro-machining systems offer important advantages and also flexibility in their manufacture. The achievable accuracy with state-of-the-art laser micro-machining systems can be better than 4 µm and thus is becoming comparable to what can be attained employing photolithography [29]. The production costs can be reduced, too, with the use of laser direct fabrication of THz devices as it will be possible to avoid post-processing steps. The attractive capabilities of laser micro-machining systems, such as non-contact 3D processing and abilities to structure directly metallic substrates, can also underpin the development of novel THz device's designs.

However, the laser micro-machining technology still has some inherent limitations that can affect the manufacturing process and thus the performance of THz mesh filters. In particular, the tapering effect on structure's sidewalls is a challenge that limits the achievable geometrical and dimensional accuracy in producing through structures [30, 31] and thus the achievable aspect-ratios in producing the functional features of THz mesh filters. Most of the THz mesh filters fabricated by laser micro-machining so far were produced using relatively thin substrates (a thickness of less than 50 µm) [32, 33] and therefore the tapering effect had a relatively small impact on their dimensional accuracy. The thermal side effects, such as the heat affected zone and the formation of recasts around the features, have been the other issues that have affected negatively the achievable accuracy when micro structures have to be produced [34]. Furthermore, laser micro-machining systems are more suitable for producing small batches of components. However, in general, it is a scalable technology that with some process setting

up automation can be made suitable for a serial manufacture, too. For example, this can be achieved by developing specialised work-holding devices [35] and capitalising on the latest advances in ultra-short pulse technology, both on constantly increasing the average power of femtosecond laser sources and optical solutions for beam splitting and shaping [36].

Taking into account the advantages and limitations of laser-based micro-machining, this research reports a feasibility study in the use of this technology for producing THz devices, especially THz mesh filters. The specific objective is to investigate the capabilities of a novel laser micro-machining technology, called precession laser micro-machining, for producing cross-shaped, free-stranding THz mesh filters out of metal materials directly without requiring any dielectric substrates. We also choose to demonstrate the capability of lasing processing by machining a 'thick' mesh filter structure [10] which presents additional fabrication challenges. In particular, a precession module was integrated into a reconfigurable workstation to control the incident angle of the laser beam. In this way, it was possible to control the beam incident angle and thus to minimise and potentially eliminate the negative tapering effect on accuracy of micro structures. The feasibility study was conducted by manufacturing THz mesh filters with different dimensions and aspect-ratios for their critical features, and thus to demonstrate the capabilities of this novel laser micro-machining process. As a reference for comparison purposes, another recently reported approach for minimising the tapering effect, called two-side laser micro-machining [37], was employed to fabricate the same THz mesh filters. The geometrical and dimensional accuracy together with the respective performance of produced filters were analysed and conclusions made about the capabilities of the proposed manufacturing approach.

Table 1. A comparison of manufacturing capabilities of laser-based and photoresist-based micro-manufacturing technologies [38].

Manufacturing solutions	***Photoresist-based***	***Laser-based***
Geometrical complexity	*2.5D*	*3D*
Requirement for secondary processes	*Mask production; Coatings*	*No*
Assembly operations	*Required*	*No*
Material requirements	*Photoresists*	*No limitations*
Vulnerability to design changes	*High*	*Low*
Environment impact	*Chemical usage*	*No*
Process flexibility	*Low*	*High*

2. Materials and methods

2.1. Cross-shaped terahertz mesh filters

Two designs of terahertz mesh filters were used to investigate the manufacturing capabilities of the proposed laser precession micro-machining method. Both filters were designed to allow frequency of 0.3 THz (300 GHz) to pass through them. The first mesh filter design (Design 1) is a single-pole filter that transmits only one peak frequency, while the second mesh filter design (Design 2) is a two-pole filter with increased frequency selectivity. The difference in their required transmission performance leads to differences in the dimensions of these two filter designs. In general, the functional feature of the two filters are arrays of cross-shaped through holes with dimensions as shown in Fig. 1. The sidewalls of the cross-shaped holes are normal to the mesh filter surface. In particular, Design 1 includes an array of 14×14 cross-shaped holes that cover a square area of 8.65 mm × 8.65 mm, while Design 2 is an array of 28×28 holes that covers an area of 26.21 mm × 26.21 mm. The designed thickness of the

two THz mesh filters is also different, 300 and 670 µm for the single-pole and the two-pole filters, respectively. Taking into account the sizes of the cross-shaped holes and the thicknesses of the substrates, the aspect-ratios that have to be achieved are 1:4.76 and 1:2.18 for Design 1 and Design 2, respectively.

99.9% purity copper was chosen as a substrate material. Copper has a very low resistivity and therefore the need for any coatings will be minimised or even eliminated. Additionally, the copper substrates are sufficiently rigid and therefore no reinforcement is required, too. This is another advantage of THz filters machined from copper substrates compared to the photoresist-based manufacturing approaches as any risks from damage during storage, transportation and installation can be reduced and even fully eliminated.

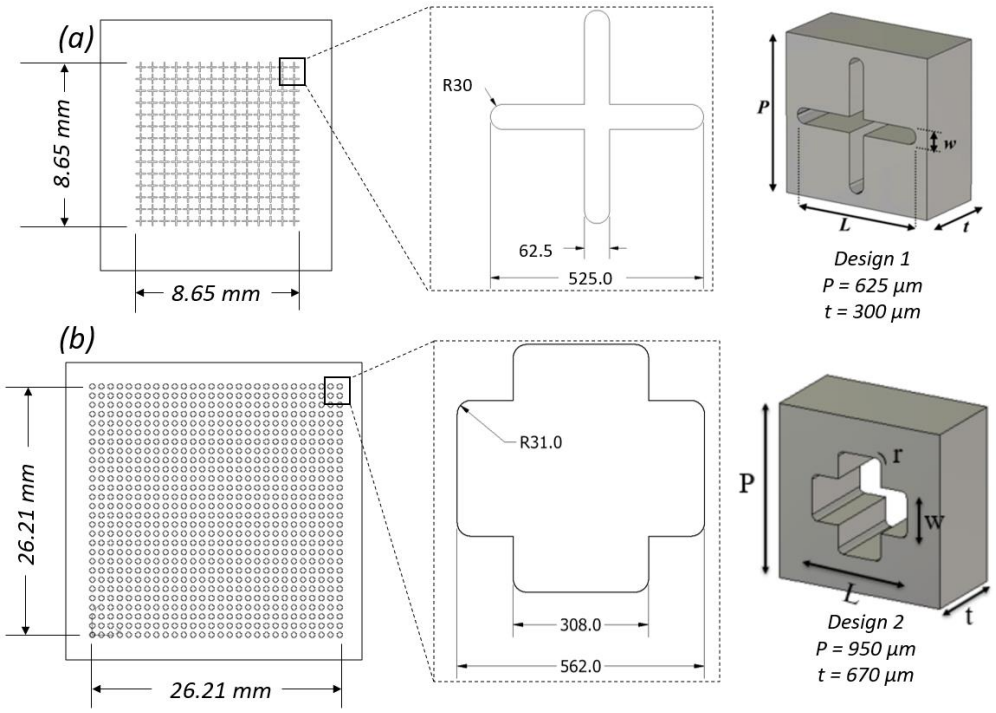

Figure 1. The two THz mesh filter designs: (a) Design 1 and (b) Design 2.

Note: the dimensions of cross-shaped holes are given in micrometers and P is the hole's preriodicity, L – the hole's length, w – the hole's width, R – the fillets' radiusm at the hole's corners and t – the thickness.

2.2. Laser micro-machining system

The THz mesh filters were fabricated using a LASEA LS-4 workstation that integrates a sub-picosecond laser source, YUJA from Amplitude Systemes, with wavelength of 1030 nm and pulse duration of 390 femtoseconds for athermal/"cold" processing. A schematic representation of the laser micro-machining setup is provided in Fig. 2. The maximum average laser power after the focusing lens was 8W and thus the pulse energy was 80 µJ at a repetition rate of 100 kHz. By using the maximum average power available, the highest possible material removal rate was used to minimise the processing time. An ultrafast laser processing was preferred in this research in order to produce mesh filters with high dimensional accuracy and quality [39]. A quarter waveplate was integrated into the beam delivery sub-system to carry out the machining with a circularly polarised beam and thus to achieve an even ablation at the focal plane [40].

The beam delivery sub-system consists of two modules, i.e. LS-shape and LS-precess. The LS-shape module is used to condition the beam and control basic laser beam properties, in particular the laser power and beam diameter. The LS-precess module is critical for realising a precession laser processing. Especially, the module allows a parallel offset and rotation of the laser beam about the beam central axis with a maximum speed of 30,000 rpm (more details are provided in Section 2.3). The laser beam is then steered with X and Y deflectors before the focusing telecentric lens with focal length of 100 mm and thus to achieve beam spot size of approximately 30 µm at the focal plane. The workpiece is placed on a stack of X and Y direct-drive linear stages with accuracy of ±1 µm and repeatability of ±0.4 µm. Each individual cross-shaped hole was machined by using only the X and Y beam deflectors while the mechanical stages were used to reposition the beam for machining the arrays of holes. Therefore, the accuracy and repeatability of the stages was important in ensuring the required periodicity between cross-shaped holes. A fume extractor was used to evacuate any debris from laser-material interaction area and thus to minimise the contamination of the machined copper substrates.

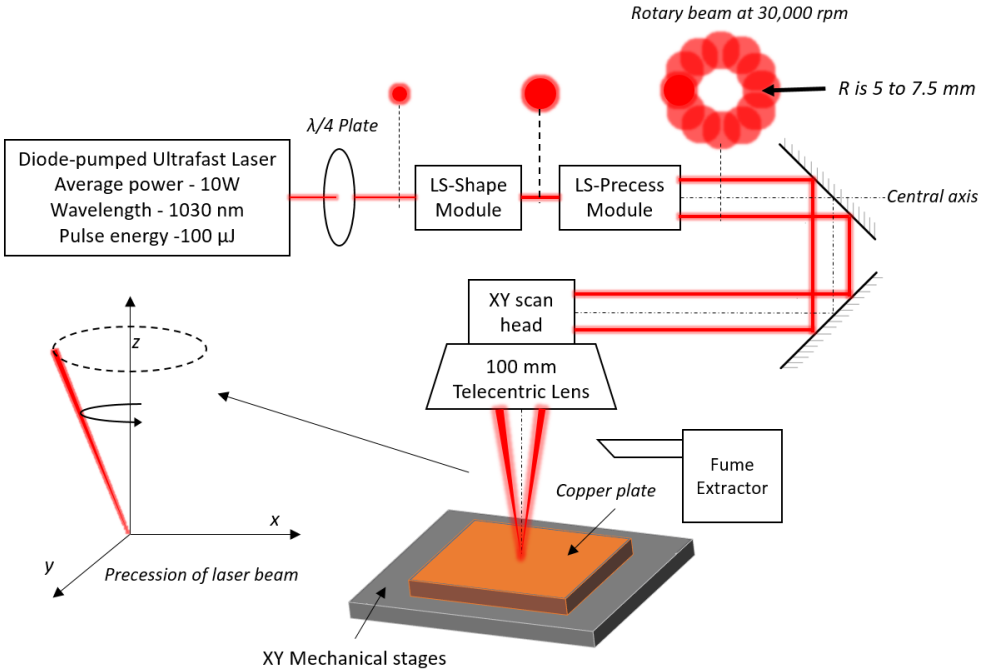

Figure 2. A schematic representation of the laser micro-machining setup.

Note: R is the beam offset from the central axis.

2.3. Precession laser machining

The LS-precess module allows a beam offset in the range from 5 to 7.5 mm while the beam remains parallel to the original central axis [41]. Then, the laser beam is rotated at high speed (up to 30,000 rpm) to create a donut ring with a diameter from 10 to 15 mm after the LS-precess module. The precession movement of the laser beam after the focusing lens is created by focusing the donut ring with a telecentric lens as depicted in Fig. 3. When the beam is offset and parallel to its central axis, the angle between the approaching beam and the first surface of the telecentric lens is no longer normal. Consequently, the output beam approaches the workpiece surface with a controllable attack angle (Fig.3a). The attack angle with the used LS-precess module can be varied from 2.9 to 4.3 degree and depends on the size of the donut ring before the focusing lens. However, there is another constraint associated with the scan head aperture, especially the maximum diameter of the donut ring is limited by the aperture

size (20 mm in the used experimental setup). Therefore, the diameter of the donut ring was kept at 12 mm approximately and thus to maximize the attack angle while avoiding any potential clipping of the rotating laser beam at the scan head aperture. This resulted in a beam attack angle of 3.46 degree after the telecentric lens. The advantages of using an incident beam that is not anymore normal to the focal plane and at the same time rotates at high speed are to ablate the material at the holes' sidewall more efficiently. This is very important when high aspect ratio structures have to be produced and the evacuation of the ablated material becomes much more difficult. Using this technique, through structures with vertical sidewalls or even a negative taper angle can be produced as shown in Fig.3b.

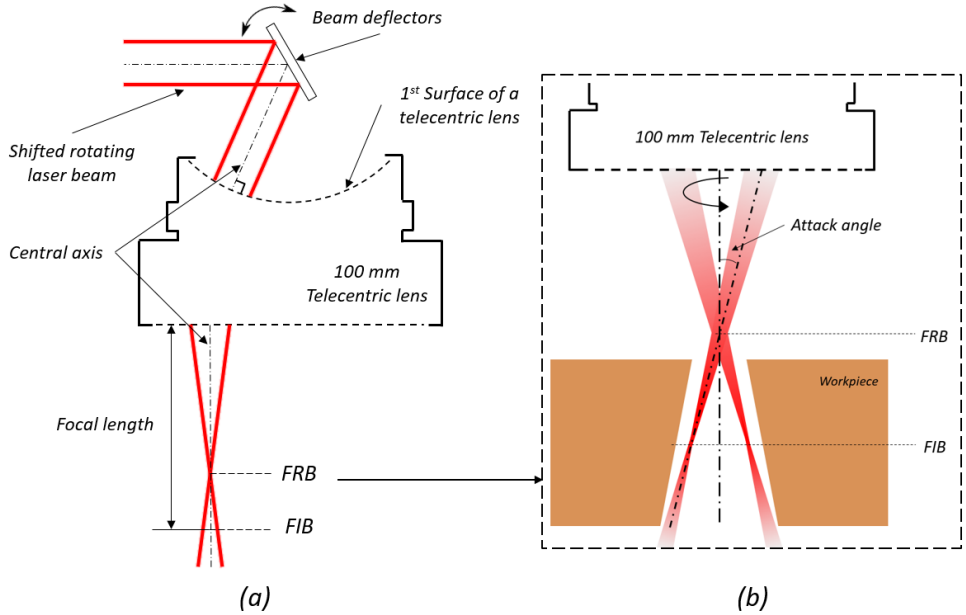

Figure 3. A schematic representation of laser beam precession movements: (a) the precession movement of the laser beam created by focusing the rotating beam, (b) zero or negative tapering effect achievable with a precession laser beam.

Note: FIB - the focus of the "individual" laser beam at the focal plane of the telecentric lens; FRB – the intersection point of the rotating beam that is along the central axis.

The cross-shaped holes of the THz filters were fabricated by employing a precession laser beam. The scanning speed of the laser beam is synchronised with its rotational speed and therefore has to be reduced significantly compared to the speeds normally used when a precession movement is not required. Especially, the scanning speed should be less than 50 mm/s during precession processing and thus to achieve a sufficient overlapping between the beam loops and so to ablate the material efficiently along the structure profiles. This is the main limitation of the precession laser processing technology. However, it is feasible to increase the scanning speed by increasing simultaneously the beam rotational speed as there is a linear interdependence between them.

A layer-based machining strategy was used to produce the cross-shaped holes. Two different scanning speeds were used to achieve an efficient material removal and produce holes with smooth edges. In particular, by trials, two scanning speeds were selected, 20.5 and 12 mm/s, and the resulting beam paths are presented in Fig.4. Nine passes with the faster scanning speed were required to achieve good overlaps between the pulses and the beam loops and to machine the copper substrates, efficiently, and remove most of the material. Then,

additional four finishing passes with the lower speed were necessary to clean the holes' edges/kerfs and also to reduce further the taper angle on the sidewalls. The use of the slower scanning regime allowed the striation effects at the holes' edges to be eliminated, especially by reducing the distance between the precession beam loops. Thus, it was possible to produce cutting kerfs with straight and well-defined edges by employing two scanning regimes.

In addition, the initial trials had shown that the scanning direction of the precession laser beam affected the edge quality. Therefore, the outer part of the precession loops was along the edges of the holes as shown in Figs 4a and 4b and as a result structures with well-defined and smooth edges were produced. Finally, the conducted trials have also shown that the cross-sectional profile of the holes should be outlined three times per layer to facilitate a proper material evacuation with the increase of the hole's depth. Especially, the holes' kerfs were widened by conducing three outlining cuts per layer with a step-over distance between them of 50 um as shown in Figs. 4c and 4d and Figs. 5a and 5c.

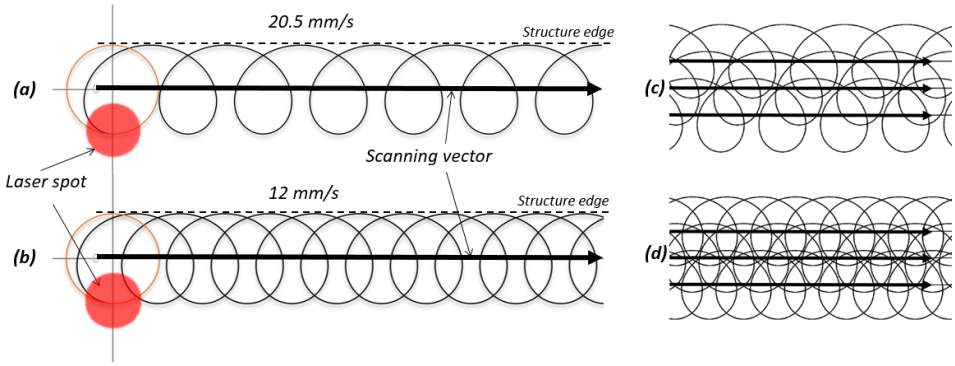

Figure 4. The beam paths for the two different scanning speeds: (a) a single pass with the faster scanning speed, 20.5 mm/s; (b) a single pass with the slower scanning speed, 12 mm/s; (c) multiple passes with the faster scanning speed; and (d) multiple passes with the slower scanning speed.

So, the precession machining strategy implemented for producing the two filter designs required three outlining cuts and each of them included nine passes with the higher scanning speed and four more with the lower speed, hence thirteen passes per cut and thirty-nine ones in total for each layer. FIB was kept at the top surface of the substrate at the start of the machining cycles and then moved down 100 μm at each layer. Three layers were required for the Design 1 filter while six layers were necessary to produce the Design 2 as showed in Fig. 5b and 5d.

The final step of the fabrication process was the cleaning of the samples in an ultrasonic bath with acetone for 10 minutes. This step was necessary in order to remove any debris inside the cross-shaped holes that can affect the performance of THz filters.

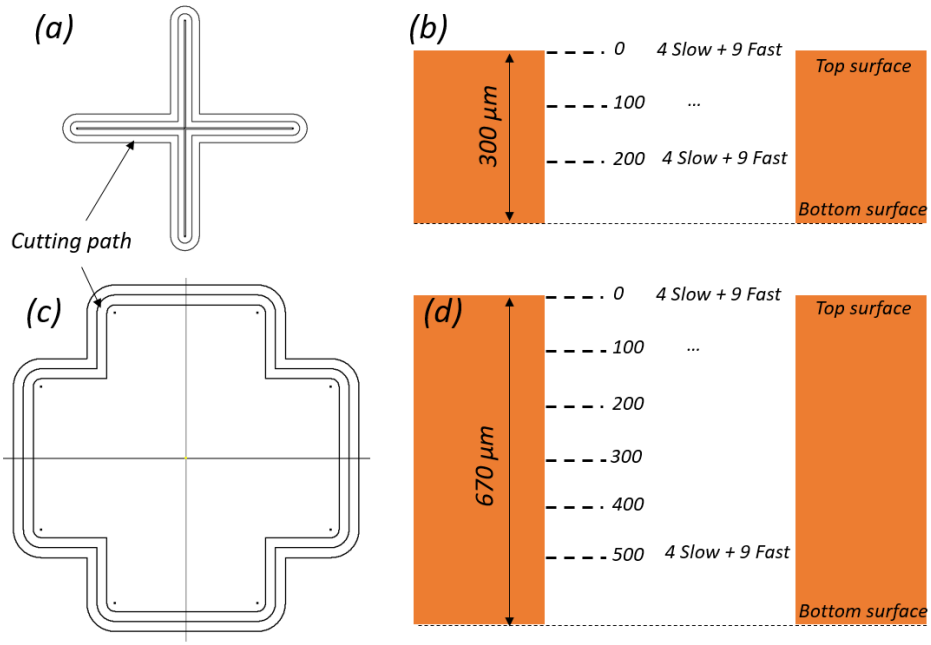

Figure 5. The layer-based machining strategies used to produce the cross-shaped holes: (a) and (c) the three cutting paths with a step-over of 50 µm used to machine each layer of the single-pole and two-pole filters, respectively; (b) and (d) the layers per cut with their 4 slow and 9 fast passes required in machining the holes of the single-pole and two-pole filters, respectively.

2.4. Two-side laser machining

As it was stated, the two THz filter designs were also fabricated using the two-side laser processing method proposed by Nasrollahi et al. [37]. The samples fabricated with this method were used as references and their performance was compared with the filters produced using the precession machining regime. Again, an ultrafast (femtosecond) laser source was used to produce the filters while the same circular polarization, 100 mm telecentric focusing lens and mechanical stages as those used in implementing the precession machining method were utilised. Especially, a mechanical rotary stage with accuracy of 29 µrad was employed to rotate the workpiece at 180 degree as required by the two-side method. Trials were conducted to find a suitable processing window for machining the filter holes with a comparable edge definition and dimensional accuracy to those achieved with the precession method. The maximum pulse energy was set at 80 uJ and achieve an accumulated fluence of 8.2 J/cm^2. In addition, a hatching strategy with a step-over distance of 10 µm was deployed to produce the holes. The pulse repetition rate was kept the same, 100 kHz, as in the precession method while the maximum possible scanning speed, 2000 mm/s, was used in order to minimise the processing time.

2.5. Measurements

2.5.1. Dimensional measurements

Dimensional analysis was carried out by using a focus variation microscope, ALICONA G5. The critical dimensions of the two filter designs were analysed. In particular, the length and width of the cross-shaped holes, the taper angle at the sidewalls and the holes' periodicity (the distance between holes) were measured.

The dimensions of cross-shaped holes were measured at nine different places over the machined areas and the average values were used to analyse the accuracy and repeatability achieved in the laser machining operations. The three-dimensional profiles/morphology of the cross-shaped holes was reconstructed by conducting focus variation measurements and thus to establish the taper angle on the holes' sidewall.

The thickness and the surface roughness of as-received substrates before the laser machining operation were also measured as they are factors affecting the performance of THz filters. The results of these measurements are provided in Table 2.

Table 2: The as-received thickness and surface roughness of the substrates used to produce the filters with the two laser micro-machining methods.

THz mesh filter design	***Design 1***		***Design 2***	
	Sample 1	***Sample 2***	***Sample 3***	***Sample 4***
Method	*Two-side*	*Precession*	*Two-side*	*Precession*
True thickness (µm)	*290-320*	*280-310*	*640-660*	*650-670*
Surface roughness S_a (µm)	*0.817*	*0.641*	*0.501*	*0.879*

Notes: the thickness of the substrates was measured with a calliper while their surface roughness with the Alicona G5 system

2.5.2. Performance measurements and simulations

The functionality of the THz mesh filters was assessed with a free space Quasi-Optic system that employs a vector network analyzer (VNA), illustrated in Fig.6. It covers the range of 220 GHz to 325 GHz in this measurement [10, 42]. The performance of THz mesh filters was assessed by measuring S-parameters that characterize their reflection and transmission in the frequency domain [43]. In particular, the S11 parameter designates the impedance matching of the filter while the S21 parameter assesses the insertion loss of the signal when it passes through the frequency selective component. These parameters are measured in decibels [dB]. An ideal THz mesh filter should transmit a wave signal at 300 GHz with a zero insertion loss.

The filters' performance was simulated by using the CST MICROWAVE STUDIO® software [44]. The electric and magnetic walls were chosen to be the opposite boundary pairs in order to model the unit cell. The resonant frequency of the unit cell was calculated by employing the full Floquet modal expansion and periodic boundaries. The efficient electric conductivity was calculated and included into the simulation [45]:

$$\sigma_{eff} = \frac{\sigma_0}{K_{SR}^2}$$

where σ_0 is theoretical electric conductivity of smooth surface material (5.87×10^7 S/m) and K_{SR} is surface roughness correction factor.

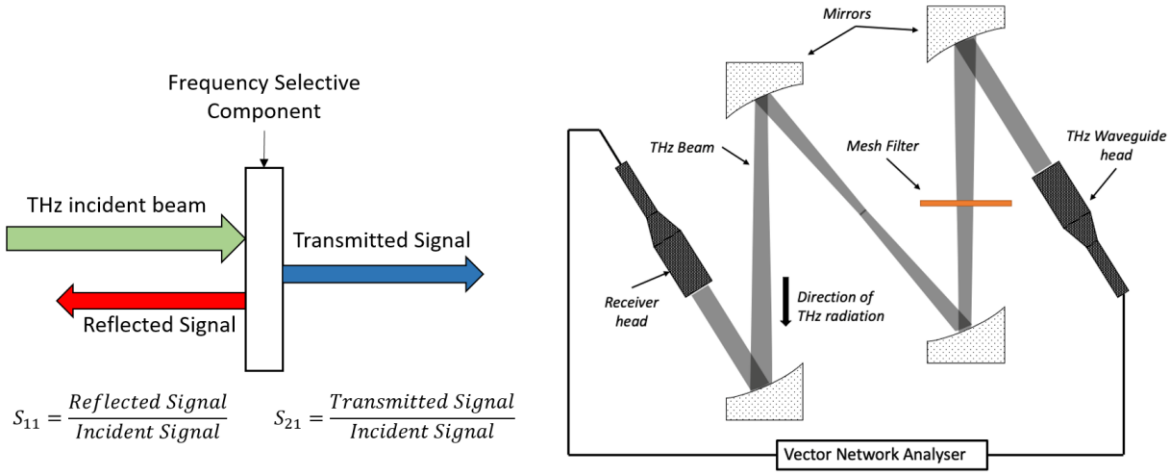

Figure 6. A schematic representation of a frequency selective components with respective S11 and S21 parameters (Left) and a schematic diagram of the free space Quasi-Optic system used to assess the THz mesh filter's performance (Right).

2.5.3. X-ray photoelectron spectroscopy analysis

X-ray photoelectron spectroscopy (XPS) analysis was performed on a Thermo Fisher Scientific K-alpha$^+$ spectrometer. Samples were analysed using 100 µm spot mode of a micro-focused monochromatic Al x-ray source (14 W). The data was recorded at pass energies of 150 eV for the survey scans and 40 eV for the high resolution scan with 1 eV and 0.1 eV step sizes, respectively. Data analysis was performed in CasaXPS using a Shirley type background and Scofield cross sections, with an energy dependence of -0.6.

3. Results and discussions

3.1. Dimensional accuracy

Four samples of the THz mesh filters were fabricated by employing the two laser micro-machining approaches, i.e. two-side and precession laser micro-machining, described in Section 2. Sample 1 (S1) and S2 are single-pole filters, while S3 and S4 are two-pole ones. The two-side laser machining approach was employed to produce S1 and S3 while S2 and S4 were produced with the precession laser machining method.

Representative images of the two prototype mesh filters are provided in Fig.7. In general, the ultrafast laser processing of copper substrates results in relatively clean structures with well-defined edges, i.e. neither observable re-cast at the edges nor apparent surface contaminations.

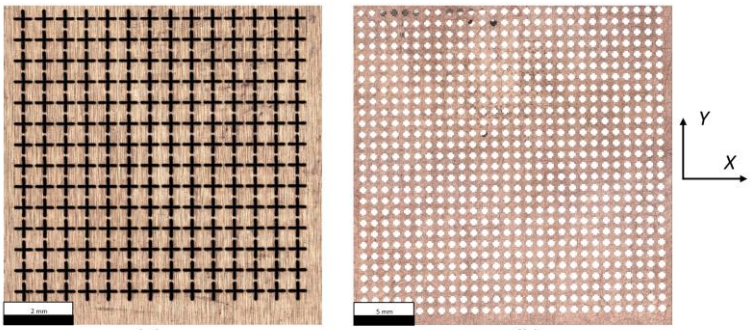

Figure 7. Representative images of the two THz filter designs produced employing the precession method: (a) Design 1 (Single-pole) and (b) Design 2 (Two-pole).

3.1.1. Taper angle analysis

The precession laser machining method led to better results with regard to the geometrical accuracy of the cross-shaped holes. Table 5 provides the measurement results, showing the reduction of the tapering effect at the sidewall in comparison to the two-side method. The average taper angle was reduced 2.6 times from 4.1 degree to 1.6 degree for the single-pole filter (Design 1). A bigger reduction of the taper angle was achieved for the two-pole filter, i.e. from 11.5 degree to 1.9 degree (6.1 times). In addition, it is important to note that this improvement was not at the expense of total machining time in spite of the fact that the precession machining process was not optimised. Especially, the machining times of S1 and S2 were the same while there was an increase of only 2 hours for S4 in comparison to S3.

Table 3: Average taper angles at the sidewalls of the two THz mesh filter designs with the machining times

THz mesh filter designs	***Design 1***		***Design 2***	
	S1	***S2***	***S3***	***S4***
Method	*Two-side*	*Precession*	*Two-side*	*Precession*
Taper angle [deg.]	*4.1*	*1.6*	*11.5*	*1.9*
Total machining time [hr]	*6*	*6*	*24*	*26*

The edge definition and the morphology of the holes produced with the two methods is depicted in Fig. 8. The sidewalls can be clearly seen in the front and back views for the holes produced with the two-side method (Fig. 8a and 8b). In contrast, the entrances (front view) were cleaner and very sharp exits (back view) were achieved on the cross-shaped holes produced with the precession laser machining method (Fig. 8e and 8f).

One of the advantages of the precession laser processing comes from the use of multiple cuts and the layer-based machining strategy. The outlining cuts in laser micro-machining have a proven positive effect on the resulting edge quality [30]. In addition, the beam precession loops in the four slow passes not only led to a further material ablation, but also helped to smooth the hole's edges. It is also important to stress that the holes were produced from one side only and the three outlining cuts with the slow and fast scanning speeds were sufficient to evacuate all ablated material efficiently. There were not visible debris or recasts at the hole's entrances. As a result, a very good edge definition at the hole's exits were achieved and there were no

evidence of a heat effected zone around them. The constructed sidewalls and extracted profiles of S1 and S2 with the focus variation method (Fig.8c, 8d, 8g and 8h) depict a clean and well-defined sidewall for the holes produced with the precession laser machining method.

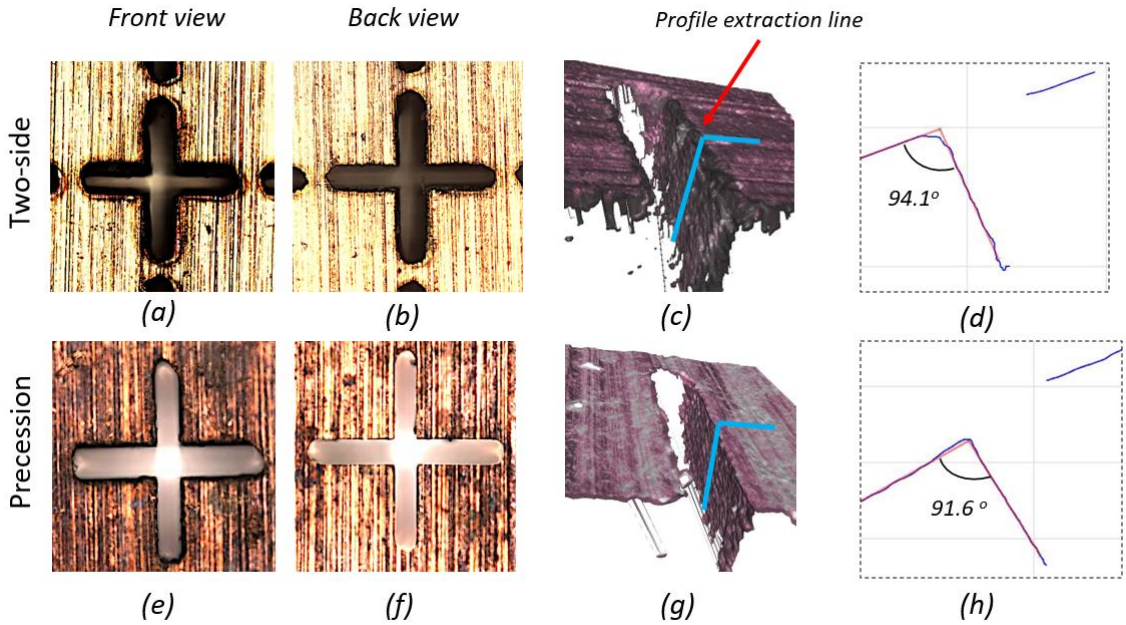

Figure 8. The cross-shaped holes of the single-pole filter fabricated by the two methods. The first row depicts a hole produced with the two-side method while the second one with the precession method, in particular: (a) and (e) the front views; (b) and (f) the back views; the reconstructed sidewalls in (c) and (g), and extracted profiles in (d) and (h).

The taper angle reduction is much more pronounced on the cross-shaped holes of the two-pole filters because the thickness of the copper substrates are more than twice higher than those used in the single pole ones. Figs. 9a and 9b depict clearly the sidewalls in the front and back views and the high taper angle and the narrowing effect in the middle of the through holes produced with the two-side method. In addition, the extracted profile in Fig. 9d shows that the taper angle increases with the increase of the depth. This results in large dimensional deviations of the hole's length and width and also a large geometrical deviation from the nominal vertical sidewalls.

In contrast, there are no apparent tapering effect on the sidewalls of the entrance and exit (Figs. 9e and 9f) of the hole machined with the precession method. This is similar to what was achieved for the holes of the single-pole filters. In fact, the taper angle decreased more than 6 times for the THz mesh filter fabricated with the precession laser beam. Furthermore, the precession method produced holes with straight walls and a consistent taper angle throughout their full depth. These is a clear evidence of the attained efficient material removal with the multiple cuts and the layer-based machining strategy. This is also evident from the uniform ablation that was maintained with the increase of the hole depth.

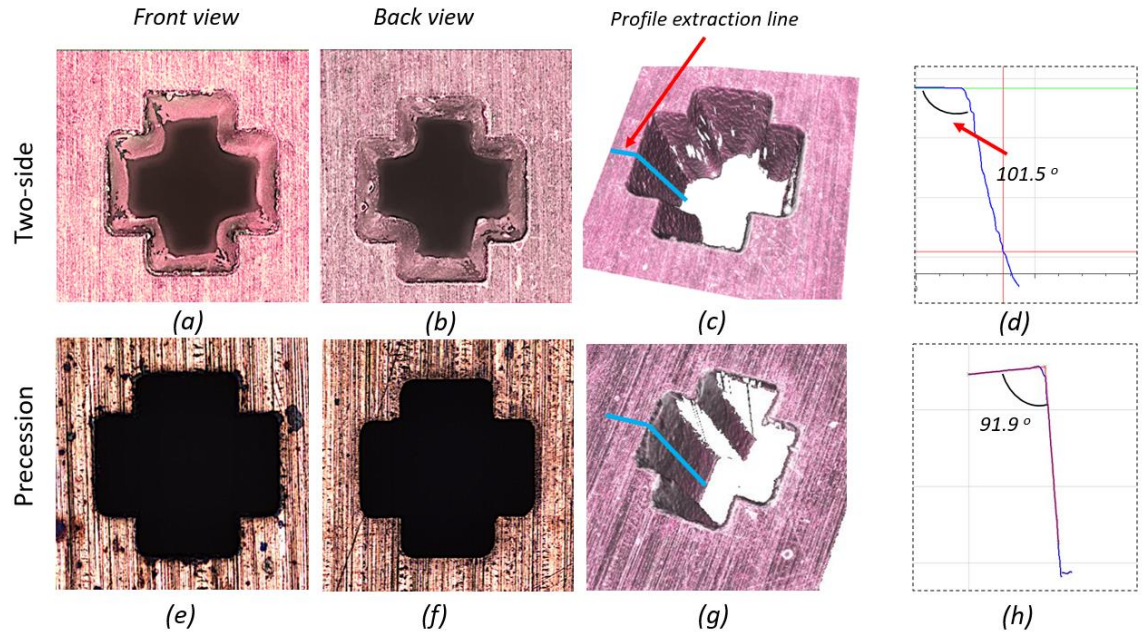

Figure 9. The cross-shaped holes of the two-pole filter fabricated with the two methods. The first row depicts a hole produced with the two-side method while the second one with the precession method, in particular: (a) and (e) the front views; (b) and (f) the back views; the reconstructed sidewalls in (c) and (g), and extracted profiles in (d) and (h).

Fig. 10 shows the cross-shaped hole's morphology obtained with by two-side method. The narrowing of the hole at the middle is an inherent issue associated with the two-side method. This is the result of the tapering effect that is common for any structure machined with a normal incident beam. This effect can be almost fully eliminated when the structurers are machined with a precession beam which leads to a significant increase of their accuracy, both dimensional and geometrical. It is worth stating that the taper angle could even be eliminated through a further optimisation of the precession machining process.

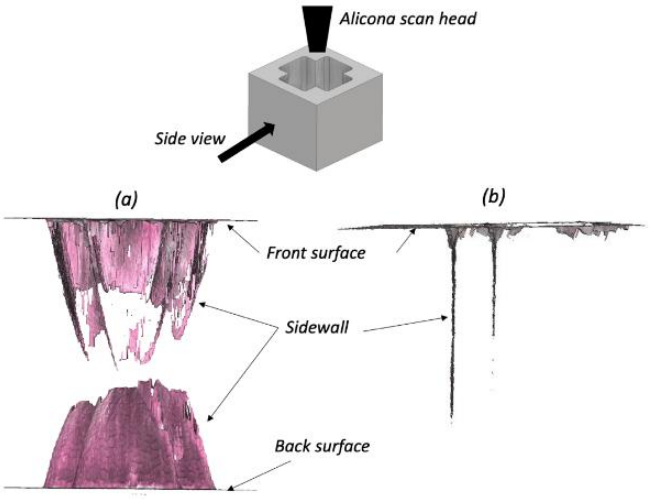

Figure 10. A comparison of hole's morphologies obtained with the two laser machining methods: (a) the narrowing effect in the two-side method; and (b) the straight vertical cuts along the hole profile produced with the precession method that define the sidewalls.

3.1.2. Dimensions in XY plane

Table 4 and Table 5 provide the dimensional measurements in both X and Y directions that includes the hole's length, width and periodicity of all samples. It can be seen in Table 3 that length and width of the S1 holes are generally bigger than those of S2 in X and Y, and also on both sides of the single-pole filter. The average deviations from the nominal dimensions on the front side were from 29 µm to 52 µm for S1 and from -1 µm to 31 µm for S2. In the case of S1, there was a slight increase of the size of the cross-shaped holes due to the relatively high aspect ratio of almost 1:5. In general, the deviations are more pronounced on the front side in comparison with the dimensional measurements obtained on the back side of the single-pole filters produced with both methods.

The results obtained on S3 and S4 were different, and they are provided in Table 5. The deviations from the nominals were higher for the two-pole filter fabricated with the precession method compared to those on the S3 filter produced with the two-side one. In particular, the average deviation from the nominal values were in the range from 84 µm to 101 µm on the entrance side and from 45 µm to 48 µm on the exit side of S4. While on S3 fabricated with the two-side method, the deviations were smaller on both sides, especially from -10 µm to 23 µm and -10 µm to 24 µm on the front and the back sides, respectively. However, the better accuracy in XY plane achieved with the two-side method did not lead to a smaller taper angle (as discussed in Section 4.1.1) or more importantly to a better filter's performance. This will be discussed in Section 3.2. In general, the variation of S2 and S4 dimensions were smaller on the exit side in comparison with the values obtained on the entrance side of the filters produced with the precession method.

The sources of errors in the two-side method were discussed in details in another research [37]. The deviation between measurements and the nominals of the filters fabricated with the precession method can be attributed to several reasons. First, the ellipticity of the laser beam played a role and has led to deviations of the dimensions in X and Y plane. In fact, the maximum difference between the biggest and smallest diameter of the laser beam was 10 µm during the machining process. This difference can be reduced by calibrating the laser beam and/or compensating this error by making adjustments in the machining strategy in X and Y directions. The second reason is the larger divergence of the focused precession beam than that of the "conventional" laser beam. Therefore, the precession beam is more sensitive to variations of the focal distance, e.g. due to any flatness deviations of the substrates used to produce the filters. The negative effects associated with this error source can be minimised by improving the quality of as-received workpieces and by employing appropriate holding devices during the machining process. The third reason is non-optimized machining strategy and processing parameters that were used to produce the filters with the precession method. In particular, the negative effects of multiple cuts and passes on dimensional accuracy in the layer-based machining strategy can be minimised by optimising the process and by introducing compensations to the X and Y dimensions. In addition, the errors associated with the used telecentric lens to focus the precession laser beam should be investigated and taken into account in optimizing the process. Finally, the repeatability of beam deflectors and the uncertainty associated with the measurements also contributed to the obtained deviations from the nominals.

The periodicity deviations from the nominal values of S1 and S2 are in the range from 0.7 to 1.3 µm and they were less than those on S3 and S4 (from 1.3 to 1.7 µm). This can be explained with the smaller number of cross-shaped holes and thus the machining fields of S1 and S2 are smaller and less prepositional movements with the mechanical stages are required. Consequently, the accumulated errors as a result of these repositioning movements are smaller. At the same time, the better periodicity obtained with the precession method can be explained with the machining of the filters from one side only and thus avoiding the alignment

error in the two-side method. It should also be noted that the cleaner and better-defined edges obtained with the precession method have reduced the uncertainty in the conducted dimensional measurements.

Table 4. Dimensional measurements of the single-pole THz mesh filters (S1 and S2) produced with the two machining methods

Dimensional measurements		Nominal dimensions [μm]	Average Value [μm]		Average deviations from nominals and standard deviation of measurements [μm]	
			S1	S2	S1	S2
Technique			Two-side	Precession	Two-side	Precession
Front side	Length X	525	554	539	29 ± 4.4	14 ± 2.2
	Length Y	525	577	556	52 ± 3.3	31 ± 3.7
	Width X	62.5	108	62	45 ± 2.9	-1 ± 3.0
	Width Y	62.5	111	77	49 ± 5.7	14 ± 6.2
Back side	Length X	525	557	520	32 ± 3.8	-5 ± 2.2
	Length Y	525	561	523	36 ± 2.2	-2 ± 3.3
	Width X	62.5	93	56	31 ± 3.7	-7 ± 1.4
	Width Y	62.5	81	64	19 ± 1.8	1 ± 3.8
	Periodicity X	625	625	625	1.3 ± 1.7	0.7 ± 0.8
	Periodicity Y	625	626	626	1.2 ± 1.3	1.2 ± 1.0

Table 5.Dimensional measurements of the two-pole THz mesh filters (S3 and S4) produced with the two machining methods

Dimension measurements		Nominal dimensions [μm]	Average Value [μm]		Average deviations from nominals and standard deviation of measurements [μm]	
			S3	S4	S3	S4
Technique			Two-side	Precession	Two-side	Precession
Front side	Length X	562	585	647	23 ± 3.1	85 ± 8.6
	Length Y	562	552	662	-10 ± 4.4	100 ± 4.7
	Width X	308	329	392	21 ± 2.3	84 ± 9.6
	Width Y	308	298	409	-10 ± 4.7	101 ± 3.6
Back side	Length X	562	586	607	24 ± 2.6	45 ± 6.3
	Length Y	562	552	610	-10 ± 3.5	48 ± 6.1
	Width X	308	330	353	22 ± 2.0	45 ± 6.6
	Width Y	308	296	355	-12 ± 4.0	47 ± 4.9
	Periodicity X	950	951	951	1.5 ± 1.9	1.5 ± 1.8
	Periodicity Y	950	950	951	1.7 ± 2.2	1.3 ± 1.5

Note: The positive values and negative values denote that the measured dimensions are larger or smaller than the nominal values, respectively.

3.2. Performance of THz mesh filters

The ultimate assessment and comparison of THz mesh filters produced with the two-side and the precession methods can be obtained by analyzing their functional performance, i.e. the S-parameters obtained with the free space Quasi-Optic system. In particular, measurement results obtained at two orientations of S2, S3 and S4 were analysed. Firstly, the filters were measured at their original orientation. Then, the filters were rotated by 90 degree to repeat the measurements. The filter's performance was analysed and recorded, again.

Fig. 11 shows the measurement results of single-pole filters fabricated with the two different machining methods. It can be seen in Fig. 11a that the S1 filter fabricated with the two-side method provide a single pole (S11 parameter) but the peak of the resonance frequency was shifted to the right of the simulation ones. Fig. 11b depicts a closer look at the S21 parameter that assesses the insertion loss of the filter, in particular the minimum loss of the S1 filter was 3.9 dB. The high-than-expected insertion loss can be attributed to the low dimensional accuracy achieved by the two-side method, especially, the narrowing effects in the middle of the S1 cross-shaped holes. In contrast, the performance of the S2 filter was much better, especially the single pole frequency (S11) was sharply defined as shown in Fig. 11c. The resonance frequency was slightly shifted to the lower frequencies in comparison to the simulation results. The offset was around 3 GHz that was equivalent to 1% error. The closer look at the S21 parameter in Fig. 11d shows a minimum insertion loss of 0.8 dB when the filter was measured at its original reference orientation. The bandwidth was also closer to the S2 simulation results.

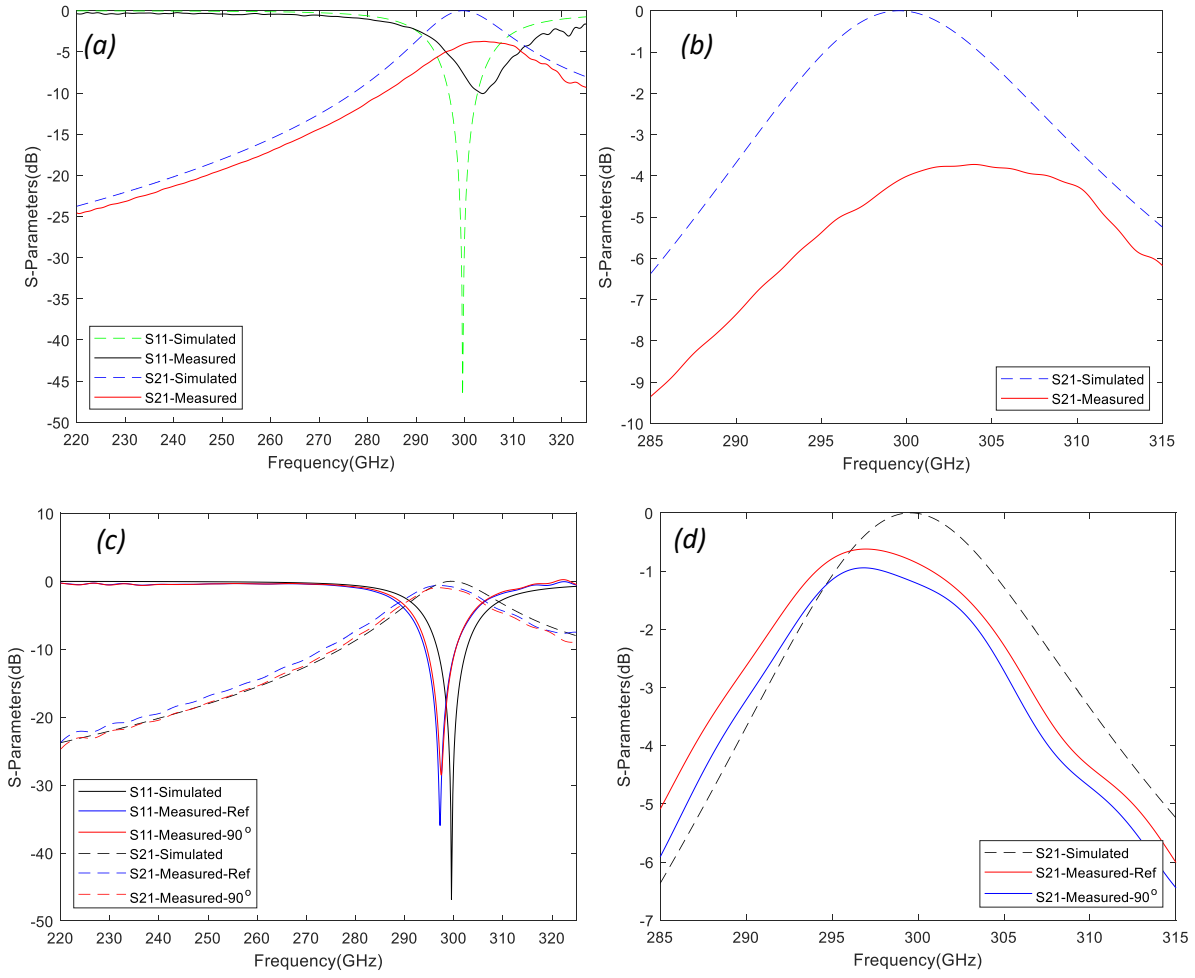

*Figure 11. The performance characteristics of **single-pole** filters: (a) S11 and S21 parameters of the S1 filter; (b) the closer look at the S21 parameter of the S1 filter; (c) the S11 and S21 parameters of the S2 filter; (d) a closer look at the S21 parameter of the S2 filter.*

The performance of the two-pole filters is depicted in Fig. 12. Again, the performance of the filter fabricated with the two-side method (S3) was not satisfactory due to the large deviations from the nominal dimensions. The S11 measurements did not show two well defined poles and there was a significant shift of 10 GHz to the higher frequency as shown in Fig. 12a. The minimum insertion loss was 4.6 dB and the bandwidth was much smaller than the simulation

results (Fig. 12b). On the other hand, the S11 and S21 characteristics of the S4 filter were in good agreement with the simulation results as depicted in Fig.12c. The two poles of the 2nd-order filter can be clearly seen and one of the poles coincides exactly with the simulated frequency of 300 GHz. The S21 measurements showed a minimum loss of 0.8 dB for both S4 orientations (Fig. 12d). In addition, the S4 bandwidth was very close to the simulation results but was slightly shifted to the lower frequencies.

It can be clearly seen that the S2 and S4 filters provided similar results with their two different orientation that indicates a consistent performance. The shifting of frequency (S11) can be attributed to the difference between designed and actual thickness of the filter [12]. Other factors discussed in Section 3.1.2 can affect the performance of the THz mesh filters, too, such as the flatness of the substrates, some oxidation of copper as a result of the laser-material interactions in not controlled environment which will be discussed next.

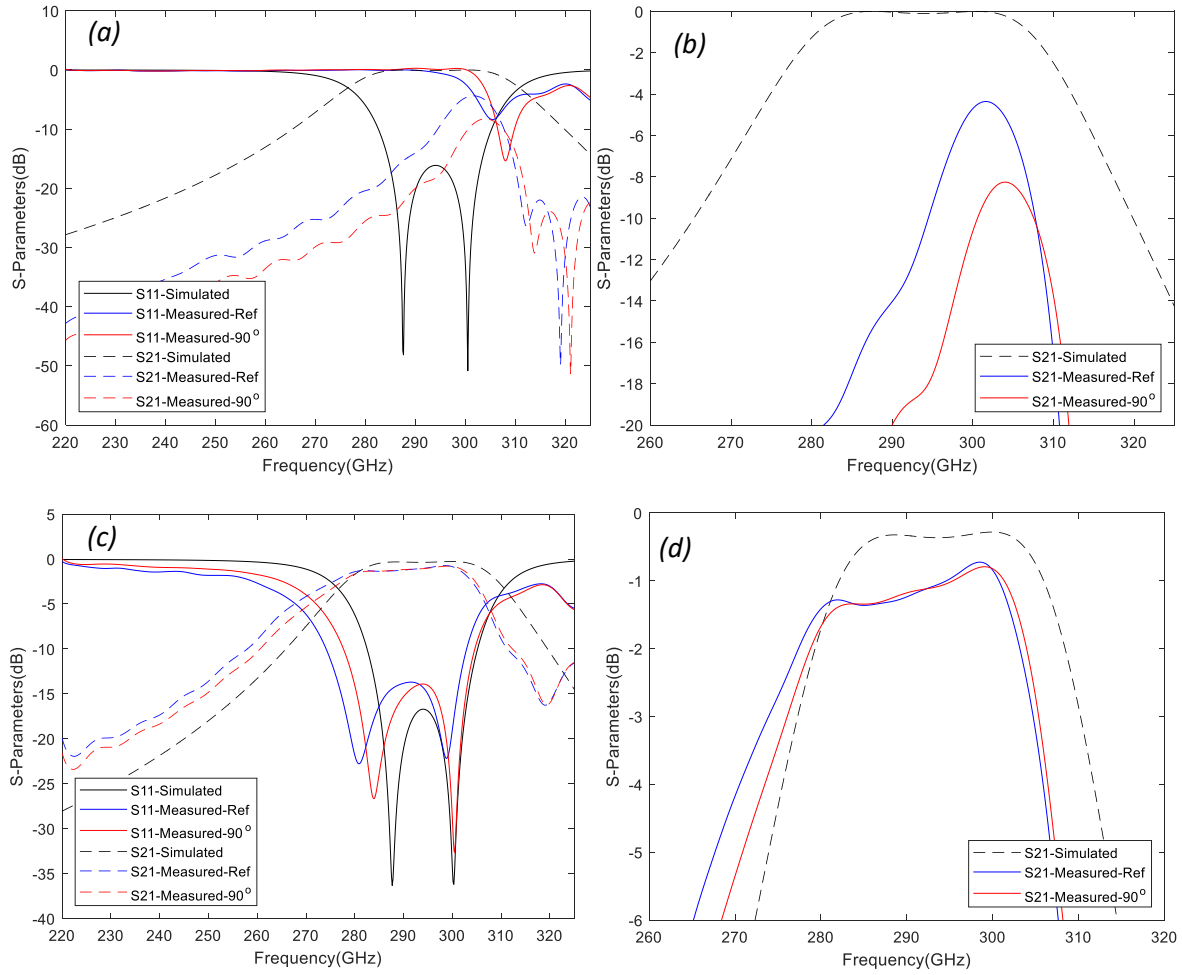

*Figure 12. The performance characteristics of **two-pole** filters: (a) S11 and S21 parameters of the S3 filter; (b) the closer look at the S21 parameter of the S3 filter; (c) the S11 and S21 parameters of the S4 filter; (d) a closer look at the S21 parameter of the S4 filter.*

3.3. HAZ and XPS analyses

An investigation of potential side-effects due to the laser machining process of copper substrates in not controlled environment was conducted as this may have negative effects on filters' performance. Fig. 13 depicts the edge of a cross-shaped hole fabricated with the two-

side and precession laser machining methods. Heat Affected Zone (HAZ) was determined by assessing the abnormal change in material colour at micro-structure's edge. It can be seen that the conventional laser machining strategy used in the two-side method did not create any HAZ, as can be expected in ultrafast laser processing. However, there are some evidences of HAZ on the hole edge after the precession machining, even with an ultrafast laser source. The HAZ appearance in the precession machining can be explained with the low scanning speeds and precession movements of the laser beam that resulted in a complex pulse overlapping and some heat load on the surface.

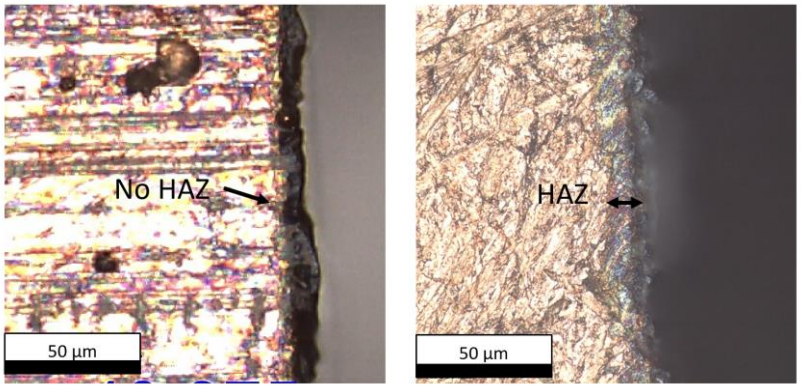

Figure 13. HAZ at the cross-shaped hole of two-pole filter design produced by Two-side technique (left) and Precession technique (right) where some material microstructure refinement is visible.

Additionally, a XPS analysis of the front side surface (unprocessed area) and the sidewall surface (processed area) of the cross-shaped holes machined with the precession method was conducted to look for potential changes in surface chemistry, especially copper oxidation. The XPS spectra in Fig. 14 and extracted atomic concentration in Table 6 show the presence of Cu 2p which signify the formation of copper oxides at both front side and sidewall surface [46]. The high-resolution normalized XPS spectra of Cu 2p (3/2 and 1/2) are depicted in Fig. 14c. The contribution of copper (I) oxide (Cu_2O) was more pronounced on the unprocessed area (the front side surface) with a peak position at around 933 eV, which indicates the formation of a native oxide layer onto the surface due to its exposure to ambient air. On the other hand, the processed area (the sidewall surface) had significant contributions of both copper (I) oxide (Cu_2O) and copper (II) oxide (CuO) components, which can be validated with the satellite features at 943 eV and the broader peak shape. This is in good agreement with the indirect ratio of oxygen/copper, which can be used to judge about the surface's oxidation level [47]. In particular, this ratio increased from 6.87 to 9.01 (calculated from Table 6) when the material was subjected to laser machining. Therefore, it can be concluded that the heat accumulation during laser precession processing of copper led to some material oxidation and this is in spite of the use of ultrashort pulses. The formation of copper oxide is undesirable and can affect the THz filter's performance because this is a non-conductive compound. Thus, the copper oxidation could contribute to the higher-than-expected insertion loss of THz filters produced by the precession laser machining method. This negative side effect can be minimised and even eliminated by conducting the laser processing in control environments.

Table 6. The composition of a copper substrate after precession laser machining

Analysed area	***Atomic concentration of found elements (%)***				
	Cu 2p (3/2)	***O 1s***	***C 1s***	***Ca 2p***	***Si 2p***
Front side	*1.79*	*12.30*	*81.51*	*0.62*	*3.78*
Sidewall	*1.28*	*11.53*	*83.39*	*1.50*	*2.30*

The analysis also showed high concentration of carbon compared to copper and oxygen. The deposition of carbon can be partly the result of contamination during the cleaning process and partly due to absorption of organic compounds in an ambient environment [48, 49]. Traces of other elements such as calcium and silicon were also identified, which could be due to some other sources of contamination, e.g. fingerprints. However, the contribution of carbon and other elements was minor and hence should not have a significant impact on the filters' functionality.

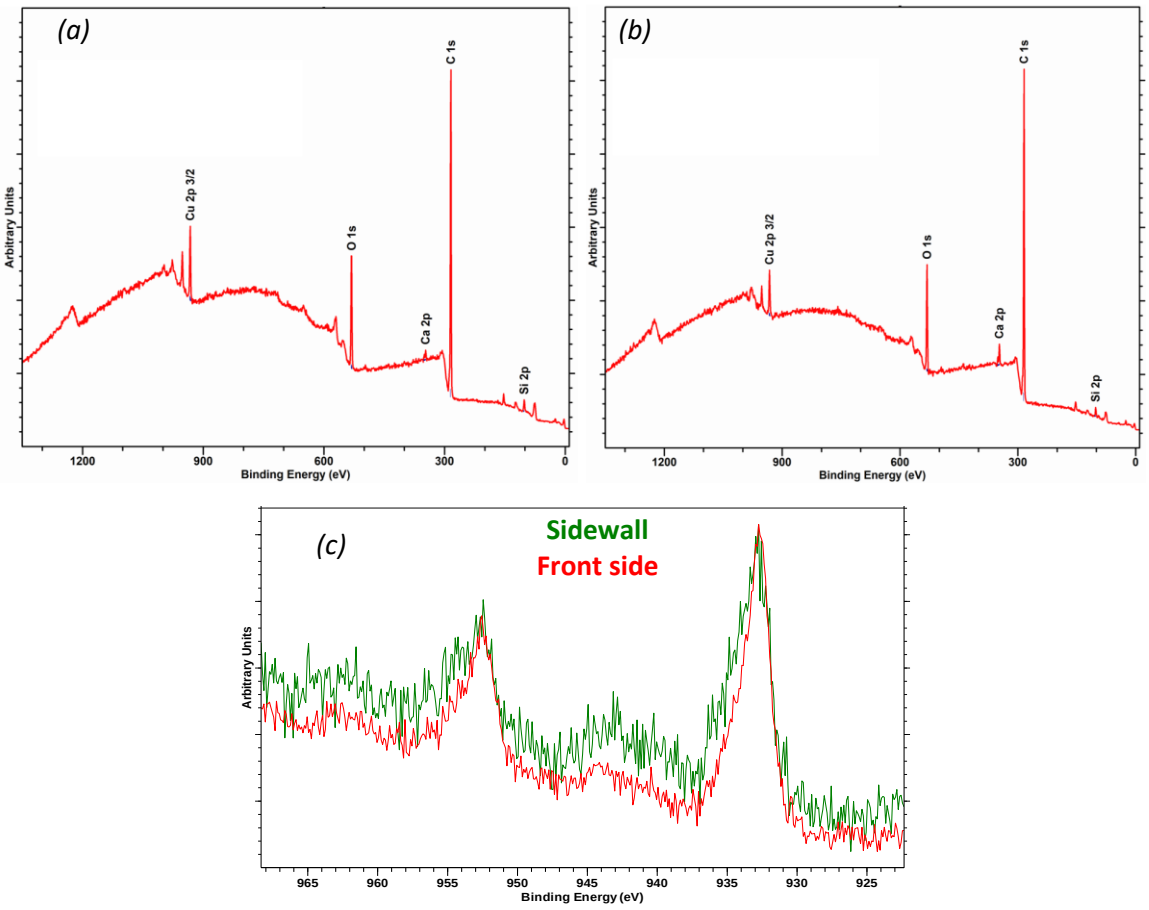

Figure 14. The XPS analysis of a two-pole filter after precession machining: (a) XPS spectra of front side surface (unprocessed area); (b) XPS spectra of sidewall surface (processed area); (c) High-resolution normalized spectra of Cu 2p as obtained for front side surface (red) and sidewall surface (green).

4. Conclusions

This study investigates a manufacturing route for producing THz mesh filters that employed a novel laser micro-machining technology, especially by machining directly relatively thick copper substrates. The method proposed in this research is called laser precession machining and it can be considered an alternative to photoresist-based fabrication technologies. Two different designs of cross-shaped THz mesh filters with thickness of 300 µm and 670 µm were successfully fabricated by laser precession machining of copper substrates. The drawback of conventional laser micro-machining processes, i.e. the tapering effect on sidewalls, was overcome by controlling the incident/attack angle of the precession process and implementing an appropriate machining strategy. In particular, the material along the cross-shaped holes of the filters was ablated efficiently by employing a layer-based machining strategy with multiple

cuts and passes at each layer and thus to reduce the taper angle on the sidewalls. In this way, it was possible to reduce the taper angle by 3 times (from 4.1 to 1.6 degree) and 6 times (from 11.5 degree to 1.9 degree) in producing the through cross-shaped holes of single-pole and two-pole filters, respectively, compared to the reference two-side method. It is important to note that this was not achieved at the expense of the machining times, which were comparable for the two methods. However, there were some relatively large dimensional deviations of the cross-shaped holes in the XY plane for the THz filters fabricated with the precession method. These can be attributed to the ellipticity of the laser beam, the sensitivity of the precession beam to any focal distance variations and the non-optimized laser precession machining process that was utilised. This shortcoming can be minimised or even eliminated by optimizing the precession machining process and by introducing some compensations to the XY dimensions in the machining strategy.

Nevertheless, the performance of the THz mesh filters that were produced had demonstrated clearly the process potential in spite of employing a sub-optimal machining strategy. The S-parameters, i.e. S11 and S21, of the single-pole filter were very closed to the simulation results, with only 3 GHz offset that is equivalent to 1% error. The two-pole filter provided two clear reflection zeros (transmission poles) while one of them was at the designed frequency of 300 GHz. The insertion loss of the filters was 0.8 dB. The loss in the transmission was mostly due to some deviations from the nominal dimensions of the machined cross-shaped holes and the formation of copper oxide at sidewall during the laser precession process. However, it is important to reiterate that this was a feasibility study and a thorough process optimisation can address the accuracy issues and improve the performance of THz mesh filters further.

Acknowledgement

XPS data collection was performed at the EPSRC National Facility for XPS (‘HarwellXPS’), operated by Cardiff University and UCL, under contract No. PR16195. The use of the 1.1 THz vector network analyser was funded by the EPSRC Strategic Equipment grant EP/P020615/1. Authors would like to thank Professor Michael Lancaster (University of Birmingham) for his supervision and doctor Stephen Hanham (University of Birmingham) for his help in measurements of the samples.

References

1. Siegel, P.H., *THz technology: An overview*, in *Terahertz Sensing Technology: Volume 1: Electronic Devices and Advanced Systems Technology*. 2003, World Scientific. p. 1-44.
2. Pawar, A.Y., et al., *Terahertz technology and its applications.* Drug invention today, 2013. **5**(2): p. 157-163.
3. Cherkasova, O.P., et al., *Effects of Terahertz Radiation on Living Cells: a Review.* Optics and Spectroscopy, 2020. **128**(6): p. 855-866.
4. Ren, A., et al., *State-of-the-art in terahertz sensing for food and water security–A comprehensive review.* Trends in Food Science & Technology, 2019. **85**: p. 241-251.
5. Nagashima, T., M. Tani, and M. Hangyo, *Polarization-sensitive THz-TDS and its application to anisotropy sensing.* Journal of Infrared, Millimeter, and Terahertz Waves, 2013. **34**(11): p. 740-775.
6. Wang, K., D.-W. Sun, and H. Pu, *Emerging non-destructive terahertz spectroscopic imaging technique: Principle and applications in the agri-food industry.* Trends in Food Science & Technology, 2017. **67**: p. 93-105.
7. Guerboukha, H., K. Nallappan, and M. Skorobogatiy, *Toward real-time terahertz imaging.* Advances in Optics and Photonics, 2018. **10**(4): p. 843-938.

8. Lindley-Hatcher, H., et al., *Real time THz imaging—opportunities and challenges for skin cancer detection.* Applied Physics Letters, 2021. **118**(23).
9. Zaytsev, K.I., et al., *The progress and perspectives of terahertz technology for diagnosis of neoplasms: a review.* Journal of Optics, 2020. **22**(1).
10. Wang, Y., et al., *Micromachined thick mesh filters for millimeter-wave and terahertz applications.* IEEE Transactions on Terahertz Science and Technology, 2014. **4**(2): p. 247-253.
11. Gavdush, A.A., et al., *Proof of concept for continuously-tunable terahertz bandpass filter based on a gradient metal-hole array.* Opt Express, 2020. **28**(18): p. 26228-26238.
12. Melo, A.M., et al., *Cross-shaped terahertz metal mesh filters: Historical review and results.* Advances in Optical Technologies, 2012. **2012**.
13. Demirhan, Y., et al., *Metal mesh filters based on Ti, ITO and Cu thin films for terahertz waves.* Optical and Quantum Electronics, 2016. **48**(2): p. 170.
14. Porterfield, D.W., et al., *Resonant metal-mesh bandpass filters for the far infrared.* Applied Optics, 1994. **33**(25): p. 6046-6052.
15. Ferraro, A., et al., *Broad-and narrow-line terahertz filtering in frequency-selective surfaces patterned on thin low-loss polymer substrates.* IEEE Journal of selected topics in quantum electronics, 2017. **23**(4): p. 1-8.
16. Wang, Q., et al., *Design, fabrication, and modulation of THz bandpass metamaterials.* Laser & Photonics Reviews, 2019. **13**(11): p. 1900071.
17. Yang, H., et al., *WR-3 waveguide bandpass filters fabricated using high precision CNC machining and SU-8 photoresist technology.* IEEE Transactions on Terahertz Science and Technology, 2018. **8**(1): p. 100-107.
18. Ao, T., et al., *Terahertz band-pass filters based on fishnet metamaterials fabricated on free-standing SiNx membrane.* Optics Communications, 2017. **405**: p. 22-28.
19. Chung, S. and S. Park, *Effects of temperature on mechanical properties of SU-8 photoresist material.* Journal of Mechanical Science and Technology, 2013. **27**(9): p. 2701-2707.
20. Puscasu, I., et al., *Comparison of infrared frequency selective surfaces fabricated by direct-write electron-beam and bilayer nanoimprint lithographies.* Journal of Vacuum Science & Technology B: Microelectronics and Nanometer Structures Processing, Measurement, and Phenomena, 2000. **18**(6): p. 3578-3581.
21. Dickie, R., et al., *THz Frequency Selective Surface Filters for Earth Observation Remote Sensing Instruments.* IEEE Transactions on Terahertz Science and Technology, 2011. **1**(2): p. 450-461.
22. Sushko, O., et al., *Comparative Study of Sub-THz FSS Filters Fabricated by Inkjet Printing, Microprecision Material Printing, and Photolithography.* IEEE Transactions on Terahertz Science and Technology, 2017. **7**(2): p. 184-190.
23. Piqué, A., et al., *Laser 3D micro-manufacturing.* Journal of Physics D: Applied Physics, 2016. **49**(22): p. 223001.
24. Voisiat, B., et al. *Laser processing for precise fabrication of the THz optics*. in *Laser Applications in Microelectronic and Optoelectronic Manufacturing (LAMOM) XXII*. 2017. International Society for Optics and Photonics.
25. Voisiat, B., et al., *Band-pass filters for THz spectral range fabricated by laser ablation.* Applied Physics A, 2011. **104**(3): p. 953-958.
26. Shang, X., et al., *W-Band Waveguide Filters Fabricated by Laser Micromachining and 3-D Printing.* IEEE Transactions on Microwave Theory and Techniques, 2016. **64**(8): p. 2572-2580.
27. Manikandan, E., et al. *Microfabrication of terahertz frequency-selective surface by short- and ultrashort laser ablation*. 2018. SPIE.
28. Born, N., et al., *Laser beam machined free-standing terahertz metamaterials.* Electronics Letters, 2015. **51**(13): p. 1012-1014.
29. Bhaduri, D., et al., *An investigation of accuracy, repeatability and reproducibility of laser micromachining systems.* Measurement, 2016. **88**: p. 248-261.

30. Le, H., et al., *Effects of Top-hat Laser Beam Processing and Scanning Strategies in Laser Micro-Structuring.* Micromachines, 2020. **11**(2): p. 221.
31. Fornaroli, C., J. Holtkamp, and A. Gillner, *Laser-Beam Helical Drilling of High Quality Micro Holes.* Physics Procedia, 2013. **41**: p. 661-669.
32. Esakkimuthu, M., et al., *Laser patterning of thin film copper and ITO on flexible substrates for terahertz antenna applications.* Journal of Laser Micro Nanoengineering, 2017. **12**(3): p. 313-321.
33. Lin, Y., et al., *Free-standing double-layer terahertz band-pass filters fabricated by femtosecond laser micro-machining.* Optics Express, 2017. **25**(21): p. 25125-25134.
34. Faisal, N., et al., *Laser micromachining of engineering materials—a review.* Micro and Nano Machining of Engineering Materials, 2019: p. 121-136.
35. Penchev, P., et al., *Generic integration tools for reconfigurable laser micromachining systems.* Journal of Manufacturing Systems, 2016. **38**: p. 27-45.
36. Martin, P.E., et al. *High-power femtosecond laser cutting and drilling combining beam-shaping and beam-splitting*. in *Laser Beam Shaping XVIII*. 2018. International Society for Optics and Photonics.
37. Nasrollahi, V., et al., *Two-Side Laser Processing Method for Producing High Aspect Ratio Microholes.* Journal of Micro and Nano-Manufacturing, 2017. **5**(4): p. 041006.
38. Penchev, P., et al., *Novel manufacturing route for scale up production of terahertz technology devices.* Journal of Micro and Nano-Manufacturing, 2016. **4**(2): p. 021002.
39. Petkov, P., et al., *Laser milling: pulse duration effects on surface integrity.* Proceedings of the Institution of Mechanical Engineers, Part B: Journal of Engineering Manufacture, 2008. **222**(1): p. 35-45.
40. Nolte, S., et al., *Polarization effects in ultrashort-pulse laser drilling.* Applied Physics A, 1999. **68**(5): p. 563-567.
41. Estival, S., P.-e. Martin, and A. Kupisiewicz, *Machining device*. 2019, US Patents.
42. Ridler, N., et al. *Traceability to national standards for S-parameter measurements in waveguide at frequencies from 140 GHz to 220 GHz*. in *2010 76th ARFTG Microwave Measurement Conference*. 2010. IEEE.
43. Horibe, M. and R. Kishikawa, *Metrological traceability in waveguide S-parameter measurements at 1.0 THz band.* IEEE Transactions on Instrumentation and Measurement, 2013. **62**(6): p. 1814-1820.
44. Jayawardene, M. and Y. Vardaxoglou, *3-D EM Simulation of Infinite Periodic Arrays and Finite Frequency Selective Horns.*
45. Hammerstad, E. and O. Jensen. *Accurate models for microstrip computer-aided design*. in *1980 IEEE MTT-S International Microwave Symposium Digest*. 1980. IEEE.
46. Long, J., et al., *Wettability conversion of ultrafast laser structured copper surface.* Journal of Laser Applications, 2015. **27**(S2): p. S29107.
47. Giannuzzi, G., et al., *Short and long term surface chemistry and wetting behaviour of stainless steel with 1D and 2D periodic structures induced by bursts of femtosecond laser pulses.* Applied Surface Science, 2019. **494**: p. 1055-1065.
48. Yang, Z., et al., *Study on the Fabrication of Super-Hydrophobic Surface on Inconel Alloy via Nanosecond Laser Ablation.* Materials (Basel), 2019. **12**(2).
49. Gaddam, A., et al., *Anti-icing properties of femtosecond laser-induced nano and multiscale topographies.* Applied Surface Science, 2021. **552**.